# Electronic structure of the tungsten (001) surface

L. F. Mattheiss and D. R. Hamann
*AT&T Bell Laboratories, Murray Hill, New Jersey 07974*
(Received 11 July 1983)

A self-consistent scalar-relativistic version of the linear-augmented-plane-wave (LAPW) method has been applied to calculate the electronic structure of an unrelaxed seven-layer W(001) slab. The results have been extended to a thicker (19-layer) film and the fully relativistic limit by means of a nonorthogonal-tight-binding (NTB) scheme that combines parameters derived from accurate NTB fits ($\sim 6$ mRy) to the bulk LAPW band structure and the seven-layer slab results. The latter fit incorporates bulk NTB parameters for the interior, relaxed bulk parameters near the surface, and additional crystal-field terms in the two outermost layers. The present scalar-relativistic LAPW and NTB surface-state bands are in good qualitative agreement with those calculated previously by Posternak *et al.* It is shown that the effects of spin-orbit coupling produce significant changes in the surface-state dispersion for $\vec{k}_{||}$ along the $\bar{\Sigma}$ or [11] direction of the surface Brillouin zone. These changes reduce the serious discrepancy that exists between the calculated scalar-relativistic surface-state dispersion curves along $\bar{\Sigma}$ and those determined in recent high-resolution angle-resolved—photoemission-spectroscopy studies.

## I. INTRODUCTION

A recent self-consistent, scalar-relativistic, linear-augmented-plane-wave (LAPW) calculation of the electronic structure of an unrelaxed seven-layer tungsten (001) film by Posternak *et al.*[1] has provided a detailed mapping of the energy-dispersion curves for surface states and resonances (denoted collectively hereafter by SR) along symmetry lines in the surface Brillouin zone (SBZ). The results were found to be in general agreement with existing angle-resolved—photoemission-spectroscopy (ARPES) and field-emission distribution (FEED) data by Weng *et al.*[2] in regard to the energies and wave-function symmetry of individual SR bands. In particular, these calculations are the first to account for the well-known "Swanson hump" (SH) state,[3] which is located at the zone center $\bar{\Gamma}$ about 0.3 eV below the Fermi energy $E_F$ and known to dominate the FEED (Refs. 2 and 3) and (normal-emission) ARPES (Ref. 2) data for W(001).

Subsequent ARPES measurements,[4,5] with improved energy and angular resolution, have provided a more precise determination of the SR dispersion characteristics along the $\bar{\Sigma}$ line of the SBZ. These more-detailed empirical dispersion curves for SR bands near $E_F$ are found to differ substantially from the LAPW results in regard to both band connectivity and Fermi wave-vector dimensions $(\vec{k}_{||})_F$. The latter discrepancies are particularly significant since they remove the "nesting" features of the LAPW SR bands along $\bar{\Sigma}$ and therefore raise doubts concerning the reliability of the surface susceptibility calculations,[6] which are based on these LAPW results. They also reopen the controversy over the fundamental mechanism for surface reconstruction.[5–7]

A more recent LAPW calculation[8] has been carried out in which the surface-layer separation has been contracted by 6% from that of the bulk. This relaxation produces only minor changes in the calculated SR dispersion curves and fails to resolve this experimental-theoretical conflict.

An important implication of this experimental-theoretical discrepancy is that the LAPW slab results seriously underestimate the actual surface charge density on the W(001) surface. This raises troublesome questions concerning the intrinsic accuracy of current "state-of-the-art" surface-science computational methods and the adequacy of the local-density approximation in regard to exchange and correlation effects near surfaces. Alternatively, the measured SR spectrum may not be characteristic of a well-ordered $p(1\times 1)$ W(001) surface. This could occur if the low-temperature $c(2\times 2)$ reconstructed phase of this surface were the result of an order-disorder rather than a displacive phase transition. In that case, the nominally $p(1\times 1)$ room-temperature surface could contain randomly oriented displacements of the surface atoms, a possibility suggested by Rutherford backscattering studies.[9]

The purpose of this paper is to address these issues by means of an independent LAPW calculation of the W(001) band structure. This provides not only a useful calibration check on the previous LAPW results of Posternak *et al.*,[1] but also contains the essential ingredients for a tight-binding extension of these results to thicker slabs and the fully-relativistic limit.[10]

The LAPW phase of the present calculations has been carried out by using an independently developed[11] self-consistent scalar-relativistic[12] version of the LAPW method.[13] The formulation includes a completely general functional form for both the charge density and potential, thereby eliminating all shape approximations. The calculations have been carried out for an unrelaxed seven-layer W(001) slab geometry which is identical to that assumed in the initial LAPW study.[1]

The results of the present LAPW calculations for W(001) are in basic agreement with those of the earlier study.[1] As a result, one must consider alternative explanations for the discrepancy with experiment concerning the SR dispersion curves along $\bar{\Sigma}$. One possibility is

 

suggested by tungsten's position in the lower part of the Periodic Table, namely spin-orbit coupling. As known from Fermi-surface measurements,[14] spin-orbit effects play an important role in determining the bulk bcc W band structure and Fermi surface.[15]

The effects of spin-orbit coupling on the SR properties of the W(010) surface have been studied recently by Grise *et al.*[10] Their investigation applied a fully-relativistic nonorthogonal-tight-binding (NTB) scheme to calculate the electronic structure for a 39-layer film. The parameters for this NTB model were determined by fitting relativistic augmented-plane-wave (RAPW) band-structure results for bulk W.[16] A serious limitation of this calculation is that it fails to yield the well-known SH state at $\bar{\Gamma}$ whose $\bar{\Sigma}$ dispersion represents an important aspect of this experimental-theoretical conflict. Consequently, the results of this bulk-derived NTB model are of limited value in mapping out the details of the theoretical SR dispersion curves near $E_F$. However, these calculations do suggest the possibility of large spin-orbit-induced splittings of SR bands along both the $\bar{\Sigma}$ and $\bar{Y}$ directions of the SBZ.

In this investigation, a refined verison[17] of the Grise *et al.*[10] fully-relativistic NTB model has been applied to calculate the SR bands for a 19-layer W(001) slab. This revised scheme involves NTB fits to both the bulk and seven-layer slab scalar-relativistic LAPW band structures. In the latter fit, the bulk NTB parameters for atoms in the surface layer are allowed to relax, and additional crystal-field terms (allowed by the reduced coordination symmetry near the surface) are introduced.[17] Finally, this scalar-relativistic NTB model has been extended to the fully-relativistic limit by adding two (tungsten $5d$ and $6p$) spin-orbit parameters, the values of which have been determined from the bulk RAPW band structure.[16]

This combined LAPW-NTB scheme provides a straightforward procedure for "stretching" the seven-layer LAPW slab results to thicker films while preserving the detailed features of the first-principles results (including the SH state). Based on the results of LAPW-NTB calculations for a 19-layer W(001) film, we conclude the following: (1) the effects of spin-orbit coupling (particularly those originating from the $6p$ states) produce significant changes in the SR dispersion curves along $\bar{\Sigma}$ by causing a pronounced splitting of the nearly-degenerate even-odd pair of scalar-relativistic bands near $E_F$. (2) In the interpretation of the ARPES data,[4,5] the higher-energy SR band along $\bar{\Sigma}$ is incorrectly associated with the SH state, which, according to the calculations, disperses rapidly above $E_F$ near $\bar{\Gamma}$. (3) The even and odd branches of the ARPES data[5] along $\bar{\Sigma}$ do not correspond to separate SR bands but instead reflect the reduced symmetry of fully-relativistic wave functions which can contain both even and odd components. This last point is important because it resolves the concern raised above that the self-consistent calculations seriously underestimate the surface-state charge.

The details of the present LAPW calculations for bcc W and a seven-layer film are contained in Sec. II A. A summary of the NTB model and the procedures employed in determining the bulk and slab NTB parameters are included in Sec. II B. The principal results of these LAPW-NTB calculations are presented in Sec. III, including energy-band, charge-density, and density-of-state plots, as well as comparisons with previous calculations and experiment.

## II. COMPUTATIONAL DETAILS

### A. LAPW calculations

The initial phase of this investigation has involved the application of the self-consistent scalar-relativistic LAPW method to calculate the electronic structure of bulk bcc W as well as that for an unrelaxed seven-layer W(001) film. In the case of the thin-film geometry, the primitive cell contains seven atoms and is subdivided into muffin-tin (MT), interstitial, and surface regions. The LAPW wave function is expanded in terms of pairs of numerical radial, plane-wave, and Laue functions in these respective subspaces. The formulation imposes no shape approximations on either the charge density or potential, both of which are expanded in terms of lattice harmonics within the MT spheres, plane waves in the interstitial region, and Laue functions in the surface regions. Aside from the omission of the surface regions, the bulk LAPW calculations are carried out in a completely analogous manner.

Both the bulk and slab calculations incorporate a frozen-core approximation in which scalar-relativistic atomic charge densities are used to represent the W core ($\cdots 4f^{14}5s^{2}5p^{6}$) states. The core-charge tails outside the MT spheres, which contain $\sim 0.1$ electron for W, are treated exactly. The formulation of Posternak *et al.*[1] differs in that atomiclike calculations are carried out for "relaxed" cores. This involves an arbitrary assumption for the potential outside the MT sphere. In addition, these authors neglect the detailed shape of core-charge tails. The success of a recent pseudopotential calculation of the total energy of bulk W by Bylander and Kleinman[18] strongly supports the accuracy of the rigid core (implicit in the pseudopotential). We do not believe that the increased computational complexity of a full-band treatment of the shallow cores, which is the only rigorous way to include core relaxation, is warranted. Exchange and correlation effects are treated in the local-density approximation by using the Wigner interpolation formula.[19]

The valence-band wave functions for wave vector $\vec{k}$ are expanded in terms of linear combinations of LAPW's which satisfy the condition $(\vec{k}+\vec{G})^2 \leq 7.5$ a.u., where $\vec{G}$ is a reciprocal-lattice vector. This leads to a variational calculation involving about 40 and 50 LAPW's per W for the bulk and slab geometries, respectively.

Both calculations utilize the bulk lattice parameter $a = 5.973$ a.u. and assume nearly-touching spheres with radii $R \approx 2.5$ a.u. Within each MT sphere, the lattice-harmonic expansion of the nonspherical potential and charge-density terms includes spherical harmonics with $l \leq 4$. In the interstitial region, the Fourier-series expansion of the charge density and potential includes 321 (bulk) and 2777 (slab) plane waves, respectively. The slab (bulk) valence charge density is determined by averaging over six (eight) special points[20] in the Brillouin zone. The starting potentials have been derived from overlapping

TABLE I. NTB orbital-energy and crystal-field parameters [$E_l$ and $(ll')_n$, respectively] for bulk bcc W and an (001) slab geometry. Slab layers are subdivided into bulk ($B$), intermediate ($I$), and surface ($S$) regions (see text). The parameters are in Ry and the common reference energy is chosen so that $E_F=0$ for both the slab and bulk.

| | Bulk parameters | Slab parameters $B$ layers | $I$ layers | $S$ layers |
|---|---|---|---|---|
| $E_s$ | 0.244 898 | 0.269 706 | 0.288 554 | 0.152 415 |
| $E_p$ | 0.737 810 | 0.762 618 | 0.745 097 | 0.658 880 |
| $E_d$ | −0.027 464 | −0.002 656 | −0.006 910 | 0.019 658 |
| $(dd)_1$ | 0.014 022 | 0.014 022 | 0.014 022 | 0.014 022 |
| $(sp)_1$ | | | | 0.086 869 |
| $(pd)_1$ | | | | 0.047 884 |
| $(dd)_2$ | | | 0.003 086 | 0.003 086 |
| $(pp)_2$ | | | −0.012 829 | −0.012 829 |
| $(sp)_2$ | | | 0.051 931 | 0.051 931 |
| $(sd)_2$ | | | 0.010 793 | 0.010 793 |
| $(pd)_2$ | | | 0.057 940 | 0.057 940 |

| Matrix elements | $B$ | $I$ | $S$ |
|---|---|---|---|
| $(s/s)$ | $E_s$ | $E_s$ | $E_s$ |
| $(x/x)=(y/y)$ | $E_p$ | $E_p+2(pp)_2$ | $E_p+2(pp)_2$ |
| $(z/z)$ | $E_p$ | $E_p+(pp)_2$ | $E_p+(pp)_2$ |
| $(xy/xy)=(yx/yz)=(zx/zx)$ | $E_d+8(dd)_1/3$ | $E_d+8(dd)_1/3$ | $E_d+4(dd)_1/3$ |
| $(x^2-y^2 \mid x^2-y^2)$ | $E_d$ | $E_d+3(dd)_2$ | $E_d+3(dd)_2$ |
| $(3z^2-r^2 \mid 3z^2-r^2)$ | $E_d$ | $E_d+2(dd)_2$ | $E_d+2(dd)_2$ |
| $(s/z)$ | 0 | $(sp)_2$ | $(sp)_2+4(sp)_1/\sqrt{3}$ |
| $(s/3z^2-r^2)$ | 0 | $-(sd)_2$ | $-(sd)_2$ |
| $(x/zx)=(y/yz)$ | 0 | 0 | $4(pd)_1/3$ |
| $(z/3z^2-r^2)$ | 0 | $(pd)_2$ | $(pd)_2$ |

atomic charge densities. The calculations have been iterated until a self-consistent solution was obtained—one in which the average difference between final input and output potentials was less than 0.1 eV. This level of self-consistency in the potential is also reflected in the stability of the energy eigenvalues. In particular, the LAPW slab energy levels at the six special $\vec{k}$ points for the last two iteration cycles have been compared. For the occupied bands, the maximum change is 0.02 eV. The average shift, particularly for states near $E_F$, is typically one-fourth as large.

### B. NTB model

The results of these scalar-relativistic LAPW calculations for bulk bcc W and a seven-layer (001) slab have been fitted by means of a NTB interpolation scheme.[17] The procedure has been initiated by means of an accurate NTB fit to the bulk W LAPW band structure at 30 $\vec{k}$ points (symmetry points and lines) in the irreducible wedge ($\frac{1}{48}$) of the bcc Brillouin zone.

The approach is similar to that of Grise *et al.*[10] in that it involves a nine-orbital ($s,p,d$) basis and the two-center approximation. However, the range of the energy-overlap interactions has been limited in the present NTB model to two (rather than three[10]) shells of neighbors. In addition, the present NTB scheme includes a crystal-field term for the $5d$ orbital energy, leading to a total of 44 parameters for the bulk fit. All energy-band states with energies below $E_F+0.65$ Ry have been included in the fitting procedure, and this resulted in a final rms error $\Delta E(\text{rms})\approx 5$ mRy. These final bulk NTB parameters for W are included among the results in Tables I and II.

These bulk NTB parameters were then introduced as starting parameters in the NTB fit to the LAPW seven-layer W(001) slab band structure. This fit included slab results at 6 points ($\bar{\Gamma},\bar{X},\bar{M}$, plus the midpoints of the connecting symmetry lines) in the SBZ with energies $E\leq E_F+0.5$ Ry. With the use of these bulk NTB starting parameters, a comparison of the seven-layer slab LAPW and NTB bands in this energy range produced a maximum error $\Delta E(\text{max})\approx 230$ mRy and a mean error $\Delta E(\text{rms})\approx 43$ mRy.

The model NTB fit to the LAPW slab results was systematically improved by relaxing various subsets of bulk parameters. Initially, these adjustments were confined to the orbital energies ($E_s$, $E_p$, and $E_d$) and crystal-field terms in the surface region. As described previously,[17] the present NTB scheme includes these crystal-field contributions by means of the parameters $(ll')_n$, where $l$ and $l'$ are the usual angular-momentum quantum numbers and $n$ denotes the shell of neighbors involved [first-nearest neighbor (1NN), second-nearest neighbor (2NN), etc.]. Because of the reduced coordination symmetry of atoms at or near the surface, additional crystal-field terms can occur in this region which are not present in the bulk.

The initial variation of bulk NTB parameters was limited to 14 slab parameters and this led to a reduced mean

TABLE II. NTB two-center energy $(ll'm)_n$ and overlap $[ll'm]_n$ parameters for $n$th neighbor interactions between atoms in bulk ($B$), intermediate ($I$), and surface ($S$) layers, respectively. The energy parameters are given in Ry.

| | $(H)_1$ $B$-$B$ | $(H)_1$ $S$-$I$ | | $[S]_1$ $B$-$B$ | $[S]_1$ $S$-$I$ | |
|---|---|---|---|---|---|---|
| $ss\sigma$ | −0.111 135 | −0.106 729 | | 0.024 233 | 0.011 685 | |
| $sp\sigma$ | 0.144 031 | 0.140 130 | | −0.031 857 | −0.057 851 | |
| $sd\sigma$ | −0.122 121 | −0.102 113 | | 0.033 077 | 0.005 605 | |
| $pp\sigma$ | 0.147 468 | 0.156 646 | | −0.042 401 | −0.036 949 | |
| $pp\pi$ | −0.016 735 | −0.021 927 | | 0.001 395 | −0.004 633 | |
| $pd\sigma$ | −0.128 802 | −0.104 955 | | 0.073 406 | 0.098 268 | |
| $pd\pi$ | 0.036 297 | 0.039 018 | | −0.018 810 | −0.011 165 | |
| $dd\sigma$ | −0.110 615 | −0.107 630 | | 0.059 153 | 0.100 196 | |
| $dd\pi$ | 0.073 538 | 0.072 941 | | −0.055 272 | −0.052 258 | |
| $dd\delta$ | −0.008 965 | −0.012 773 | | 0.010 159 | −0.001 969 | |
| | $(H)_2$ $B$-$B$ | $(H)_2$ $S$-$B$ | $(H)_2$ $S$-$S$ | $[S]_2$ $B$-$B$ | $[S]_2$ $S$-$B$ | $[S]_2$ $S$-$S$ |
| $ss\sigma$ | −0.036 878 | −0.066 297 | −0.079 209 | −0.001 677 | 0.027 886 | 0.027 733 |
| $sp\sigma$ | 0.053 756 | 0.035 255 | 0.084 933 | −0.008 882 | −0.001 920 | −0.013 192 |
| $sd\sigma$ | −0.056 806 | −0.057 378 | −0.053 632 | 0.050 529 | 0.030 571 | 0.060 115 |
| $pp\sigma$ | 0.128 012 | 0.126 330 | 0.141 486 | −0.043 782 | −0.073 181 | −0.041 804 |
| $pp\pi$ | −0.017 642 | 0.006 440 | −0.059 662 | 0.007 950 | 0.026 311 | −0.026 583 |
| $pd\sigma$ | −0.085 893 | −0.080 961 | −0.071 510 | 0.059 004 | 0.008 143 | 0.065 669 |
| $pd\pi$ | 0.004 705 | 0.004 247 | 0.030 916 | −0.004 109 | 0.001 171 | 0.005 108 |
| $dd\sigma$ | −0.076 130 | −0.077 644 | −0.069 695 | 0.036 398 | 0.010 472 | 0.046 821 |
| $dd\pi$ | 0.019 486 | 0.018 733 | 0.028 759 | −0.022 379 | −0.051 953 | −0.005 389 |
| $dd\delta$ | 0.000 338 | 0.005 063 | −0.001 895 | −0.004 066 | −0.012 077 | 0.011 910 |

error $\Delta E(\text{rms}) \approx 18$ mRy. In identifying these parameters, it is convenient to subdivide the seven-layer slab into three types of layers, including two surface ($S$), two intermediate ($I$), and three bulk ($B$). These 14 initially-varied slab parameters include (1) an additive constant $\Delta$ to the $B$ orbital energies $E_l$ (to compensate for any small errors in the determination of $E_F$, the NTB reference energy, in the LAPW bulk and slab calculations); (2) six independently adjusted $I$ and $S$ orbital energies $E_l$; (3) seven additional crystal-field terms $(ll')_1$ (for $S$ atoms) and $(ll')_2$ (for $I$ and $S$ atoms) in the $I$ and $S$ layers.

The final slab-parameter variation involved the added relaxation of 60 bulk two-center energy-overlap parameters in the surface region, including 1NN $S$-$I$ as well as 2NN $S$-$S$ and $S$-$B$ interactions. This produced a final NTB fit to the slab LAPW bands with a maximum error $\Delta E(\text{max}) \approx 18$ mRy and a mean error $\Delta E(\text{rms}) \approx 6$ mRy. The quality and accuracy of this NTB fit is demonstrated by the fact that the fitting errors for only 13 out of 240 states exceed 12 mRy or 1% of the total energy range spanned by the fit. Of these, only five have appreciable NTB weight on the surface-layer atoms. However, none of these form a part of the surface-state bands that we are concerned with in this study. These final NTB slab parameters are listed in Tables I and II.

A comparison of the bulk and slab NTB parameters in Tables I and II reveals some evidence of systematic variations in the orbital energies but less in regard to the two-center energy and overlap parameters. In Table I the $6s$-$6p$ orbital energies in the outermost layer decrease by about 0.1 Ry relative to the bulk whereas $E_d$ exhibits a slight ($\sim$0.02 Ry) increase. Unfortunately, there are no obvious trends exhibited by the $S$-$S$, $S$-$I$, and $S$-$B$ two-center energy-overlap parameters in Table II that would facilitate the application of bulk parameters to surface electronic-structure calculations.

Since the NTB slab fit was restricted to a rather small number of symmetry points in the SBZ, it is important to check the overall accuracy of the NTB results at intermediate wave vectors. A test was carried out by utilizing the LAPW results at the six low-symmetry special points[20] used for evaluating the Brillouin-zone average of the valence charge density. This comparison of NTB and LAPW eigenvalues yielded essentially the same mean error $\Delta E(\text{rms}) \approx 6$ mRy.

The RAPW results of Christensen and Feuerbacher[16] for bulk W have been used to determine values for $\xi_{5d}$ and $\xi_{6p}$, the $5d$ and $6p$ spin-orbit parameters, respectively. The splittings of the (scalar-relativistic) $5d$ states with $\Gamma_{25'}$ and $H_{25'}$ symmetry imply a slightly energy-dependent $5d$ spin-orbit parameter with an average value of $\xi_{5d} = 0.0263$ Ry. This is about 10% smaller than the value determined in the previous NTB fit by Grise *et al.*,[10] where $\xi_{5d} = 0.0297$ Ry. An analysis[15] of the bulk W Fermi-surface dimensions in terms of a less sophisticated tight-binding model yielded a comparable semiempirical estimate $\xi_{5d} \approx 0.03$ Ry. The slight energy dependence of $\xi_{5d}$ is consistent with Andersen's analysis[21] of RAPW results for fcc transition metals in the latter part of the transition series.

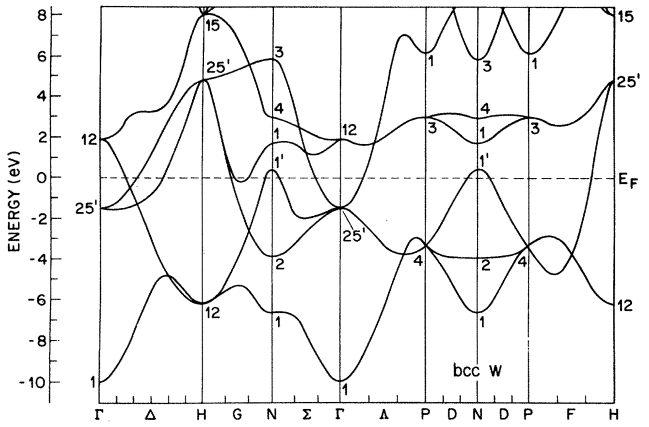


FIG. 1. Scalar-relativistic LAPW energy-band results for bulk bcc W.

A similar NTB fit to the calculated RAPW splitting of the scalar-relativistic $H_{15}$ state yields a value for the $6p$ spin-orbit parameter $\xi_{6p}=0.1262$ Ry. However, in this case, the assumption of a constant energy-independent value for $\xi_{6p}$ is less satisfactory. In particular, an NTB study of the sign and magnitude of the spin-orbit-induced splittings of the two lowest scalar-relativistic $P_4$ states implies that $\xi_{6p}$ *decreases* rapidly as a function of increasing energy (from about 0.28 to 0.04 Ry over a 1.1-Ry energy interval).

The origin of this strong energy dependence of $\xi_{6p}$ is not fully understood. Andersen's calculation[21] of $\xi_{6p}(E)$ for Pt and Ir over a comparable energy range indicates a modest (10—20%) increase in $\xi_{6p}$ with increasing energy. It is believed that the inferred increase in the $\xi_{6p}$ parameter for W at low energies is a renormalization effect which arises from the diffuse nature of the $6p$ wave function. Since the present NTB scheme[17] incorporates only energy-independent parameters, we have neglected this effect in the present NTB calculations and have used the above $H_{15}$-derived value for $\xi_{6p}$ in this study.

## III. RESULTS AND DISCUSSION

We consider first the bulk LAPW band-structure results for bcc W, since these provide a useful reference for analyzing and interpreting the results of the corresponding slab calculations. The present scalar-relativistic LAPW energy-band results for bcc W are shown in Fig. 1. A key energy-band feature that is useful for evaluating the accuracy of these results in comparison with existing Fermi-surface data concerns the position of the $N_{1'}$ state ($6p$ character) with respect to $E_F$. The present value (+0.5 eV) is in good agreement with that determined from the observed dimensions of the hole Fermi-surface sheet at $N$ (+0.3 eV).[15] (Spin-orbit coupling has a small effect on this state; its energy is reduced to +0.4 eV in the fully-relativistic NTB calculation.)

The LAPW results in Fig. 1 are in excellent agreement with those calculated recently by Bylander and Kleinman[18] using a self-consistent, scalar-relativistic pseudopotential method. The most noticeable difference between the two results concerns the relative positions of the $6s$-$6p$ and $5d$ bands. In the pseudopotential calculation, the $6s$-$6p$ bands are about 0.5 eV higher in energy relative to the $5d$ bands and $E_F$ than the present LAPW results. As a result, their $N_{1'}$ state is about 1 eV above $E_F$. This difference probably arises from the fact that the two calcula-

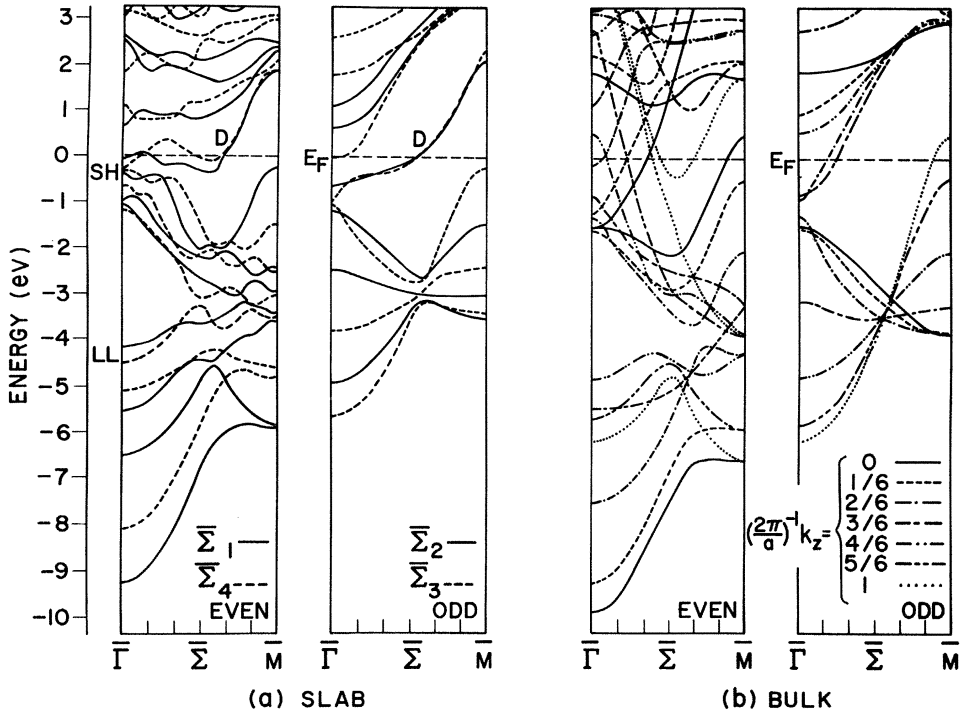


FIG. 2. (a) LAPW $E(\vec{k})$ curves along $\bar{\Sigma}$ for a seven-layer W(001) slab; (b) projected bulk bands along $\bar{\Sigma}$. States which are even and odd under (110) reflection are plotted separately.

tions incorporate different forms of the exchange potential. Previous studies[15] have shown that this feature of the W band structure is particularly sensitive to the details of the exchange-correlation contribution to the potential.

The LAPW energy-band results for a seven-layer film are plotted in Fig. 2(a) for wave vectors $\vec{k}$ along the $\bar{\Sigma}$ or [11] direction of the SBZ. Those states which are even ($\bar{\Sigma}_1$ and $\bar{\Sigma}_4$) and odd ($\bar{\Sigma}_2$ and $\bar{\Sigma}_3$) under a (110) reflection are plotted separately. It is readily shown that these ($\bar{\Sigma}_1, \bar{\Sigma}_4$) and ($\bar{\Sigma}_2, \bar{\Sigma}_3$) pairs have the proper symmetry such that sums and differences of these slab wave functions can yield states which are localized on one surface or the other. The principal SR bands in Fig. 2(a) are labeled SH, D, and LL, in accordance with previous notation.[5]

The slab energy-band results in Fig. 2(a) exhibit complicated shapes that are indicative of "crossed" bulk bands that are "uncrossed" by the reduced symmetry of the slab geometry. This is indeed the case, as the projected bulk energy-band results plotted in Fig. 2(b) illustrate. Here, we have superimposed the projected bulk bands along $\bar{\Sigma}$ for seven equally-spaced values of $k_z$ (one for each layer of the slab), again plotting the even and odd states separately. These projected bulk bands consist of a complicated array of crossed bands whose features are generally consistent with the band shapes in Fig. 2(a).

The projected bulk band-structure results of Fig. 2(b) also provide insight regarding the nature and origin of individual SR bands. Historically, these have subdivided into two categories, Tamm[22] and Shockley[23] states. Although the distinction between Tamm- and Schockley-type states is often ambiguous,[24] we can identify both the even and odd components of the SR bands labeled D in Fig. 2(a) as Shockley states. As seen from an examination of the projected bulk bands in Fig. 2(b), these highly localized SR bands remove one bulk each from both the upper and lower energy-band manifolds. Of particular interest is the fact that lower bulk band in each case is expected to have substantial $6p$ character near $\bar{M}$ since it evolves from the predominantly $6p$ bulk $N_{1'}$ state.

The remaining pair of even SR bands (SH and LL) appear to be Tamm states since they originate from shifted bulk bands that are essentially squeezed out of the same manifold. Their surface localization is due principally to differences between bulk- and surface-atom potentials. The SH state is particularly sensitive in this regard. Its energy is slightly above $E_F$ in the zeroth iteration to self-consistency, where the potential is derived from superimposed atomic charge densities. Gradually, this SH state moves below $E_F$ in subsequent iterations to its final position at about $-0.4$ eV.

Except for the well-localized even-odd doublet SR bands D, there exists some ambiguity in ascertaining the detailed shape and connectivity of the various SR dispersion curves. This is due partially to the finite thickness of the slab, which causes splittings of SR states localized on opposite faces (resonance width) and also produces a discrete density of slab states for each $\vec{k}_{||}$. Since these effects are reduced in the NTB 19-layer slab results, we shall temporarily defer a discussion of the SR dispersion curves.

LAPW valence charge-density results for W are shown in Fig. 3. The calculated charge contours for the seven-layer slab geometry are shown in Fig. 3(a). In general, these results are in reasonable agreement with those of Posternak *et al.*[1] The two principal differences concern (1) the connectivity of the "6.0" charge-density contours

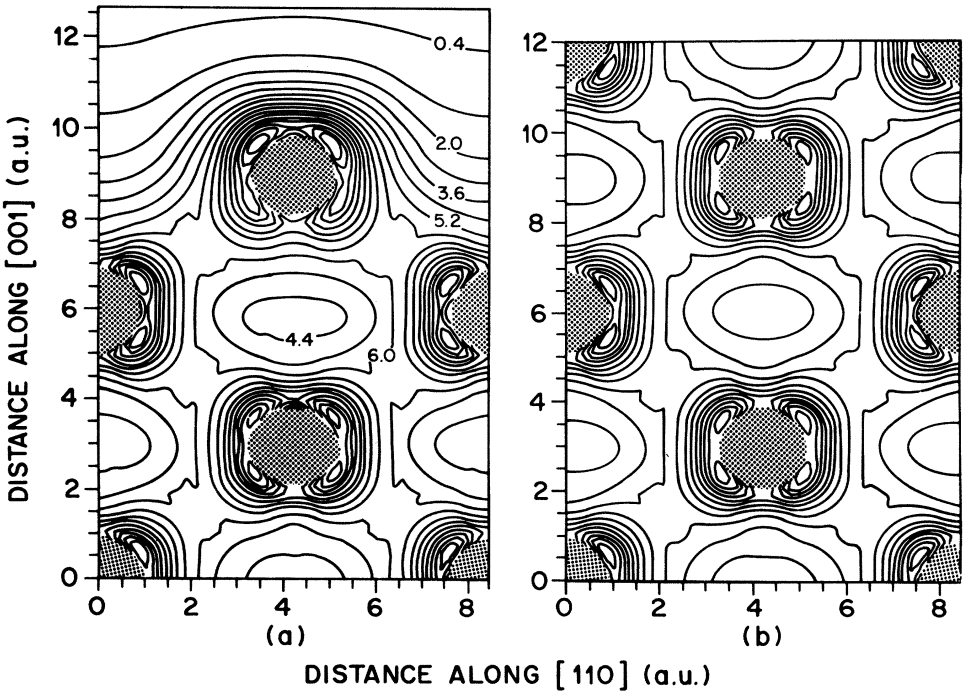


FIG. 3. Comparison between W valence charge densities derived from (a) slab and (b) bulk LAPW calculations. Adjacent contours correspond to increments of 0.8 electron per bulk unit cell.

along nearest-neighbor bond directions and (2) the depth of the charge-density minimum (i.e., the presence of "4.4" contours) along second-neighbor directions. The latter difference is probably due to the fact that Posternak *et al.* used a bulk lattice parameter of 5.793 a.u. rather than the correct value of 5.973 a.u., which would tend to produce more charge density in the interstitial region.

For comparison, the corresponding bulk LAPW valence charge-density results are shown in Fig. 3(b). These charge contours are exceedingly similar to the slab results and serve to emphasize the rapid healing of surface effects in metals as one penetrates one or two layers into the bulk.

The present LAPW calculation yields a theoretical value for the work function of the W(001) surface, $\phi=4.55$ eV. This is in good agreement with the value determined by Posternak *et al.*[1] (4.5±0.2 eV) as well as the observed[25] value (4.62 eV).

We consider now the NTB model results derived from 19-layer slab calculations. Density-of-state (DOS) curves are shown in Fig. 4. These have been calculated from the NTB bands at fifteen special points in the irreducible triangle of the SBZ. These discrete levels were then smoothed with a Gaussian function with an 0.3-eV full width at half maximum (FWHM). Separate curves illustrate the total DOS as well as individual layer-projected DOS curves for surface, first interior ($S-1$), and central W-atom planes. The layer-DOS curves have been determined by weighting the total DOS by the sums of squares of the appropriate NTB eigenvector coefficients of $H' \equiv S^{-1/2} H S^{-1/2}$, for which the overlap matrix is diagonal.[17]

These layer-projected NTB DOS curves exhibit the same general characteristics as the LAPW-derived results of Posternak *et al.*,[1] both of which were derived from results at fifteen special points. It is noted that the LAPW projections include only the integrated charge within the MT spheres in the evaluation of the layer-DOS curves.

Grise *et al.*[10] have calculated higher-resolution planar DOS curves for a 27-layer film with level sampling at 91 special points. Their results, which include spin-orbit coupling, a Mulliken analysis of overlap effects, and a substantially reduced Gaussian smoothing (FWHM≈0.04 eV), are also in good agreement with those shown in Fig. 4 for the interior layers. Significant differences in the peak structure near the Fermi level occur in the surface layer.

These differences are also present in the integrated NTB planar DOS results. In their fully-relativistic calculations, Grise *et al.*[10] find a charge deficit of 0.17 electrons/atom on the surface layer and a surplus of 0.21 electrons/atom one layer in. In the present scalar-relativistic NTB results, the corresponding surface-atom charge deficit is reduced by about a factor of 2 to 0.08 electrons/atom while the second-layer surplus is also decreased to 0.15 electrons/atom.

The NTB scalar-relativistic energy-band results along $\bar{\Sigma}$ for a 19-layer film are plotted in Fig. 5. As in Fig. 2, the even and odd states are plotted separately. It is evident that the 12 added layers serve to define the bulk band gaps more clearly in Fig. 5 in comparison with the seven-layer results in Fig. 2. However, the only clearly-recognized surface state is the odd component of the doublet D shown to the right, which falls near the middle of a gap in the odd projected bulk band structure.

The details of the SR bands and their dispersion along $\bar{\Sigma}$ are shown more clearly in Fig. 6(a). The NTB slab

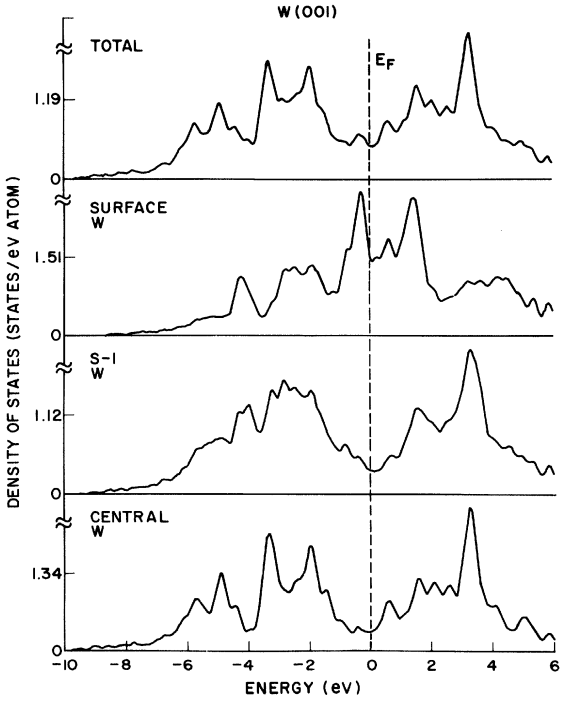


FIG. 4. NTB total and projected DOS curves for a 19-layer W(001) film (omitting spin-orbit coupling).

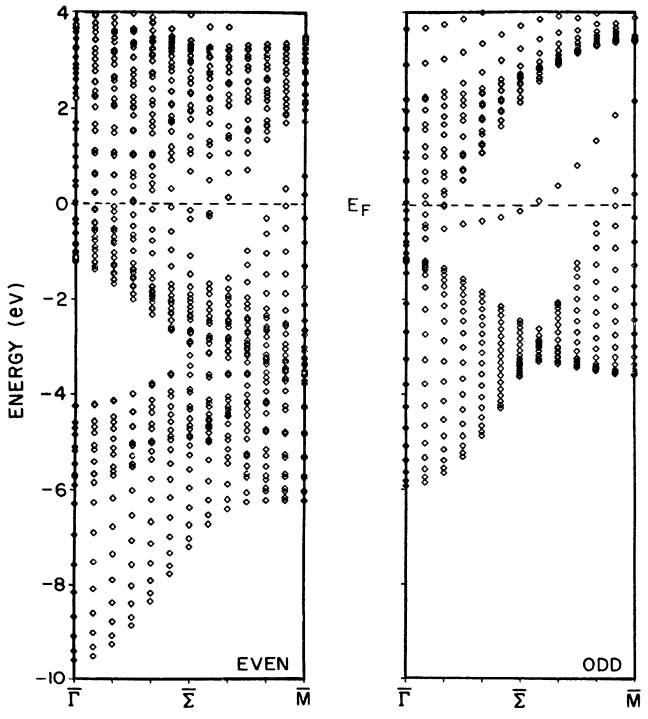


FIG. 5. NTB $E(\vec{k})$ results along $\bar{\Sigma}$ for a 19-layer W(001) film (omitting spin-orbit coupling).

states included in this plot are such that a minimum of 15% of their weight is concentrated on each of the outermost surface layers. Taking sums and differences of the indicated pair yields SR states with at least 30% weight on a single surface layer.

The odd component of the doublet D is highly localized and its dispersion is well defined over $\frac{5}{6}$ of the $\bar{\Sigma}$ line. It consists primarily of $5d$ orbitals with $(x^2-y^2)$-type symmetry, with some $(xy\text{-}yz)$ admixture. The corresponding dispersion curves for the even SR states are considerably more complicated. These consist of four distinct bands which are labeled LL, SH, D, and C, respectively. The principal orbital component of each of these even SR bands is also indicated.

The low-lying LL is well defined and extends over about one-third of the $\bar{\Sigma}$ line. The connectivity of the C, D, and SH bands is clearly defined near the $\bar{M}$ point but gradually becomes obscured as one moves closer to $\bar{\Gamma}$. The orbital character of the SH state varies rapidly for $\vec{k}_{\|}\neq 0$, and the indications are that this band disperses quickly above $E_F$, as suggested by the dashed lines. The apparent crossing of the C, D, and SH bands for $\vec{k}_{\|}$ near $\bar{\Gamma}$ causes gradual surface delocalization of each band and

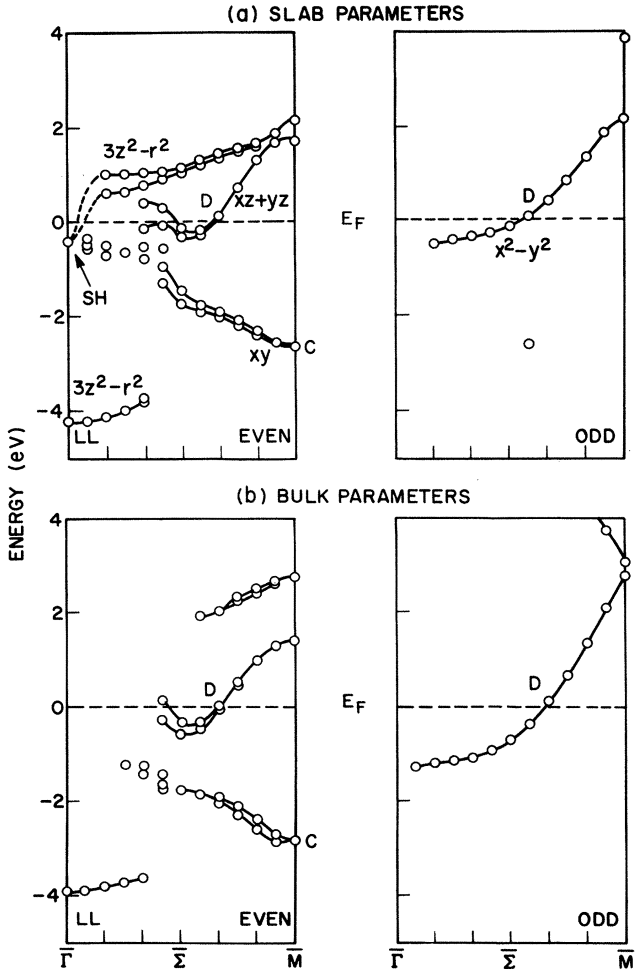


FIG. 6. Comparison of SR dispersion curves along $\bar{\Sigma}$ calculated using (a) NTB slab and (b) NTB bulk parameters.

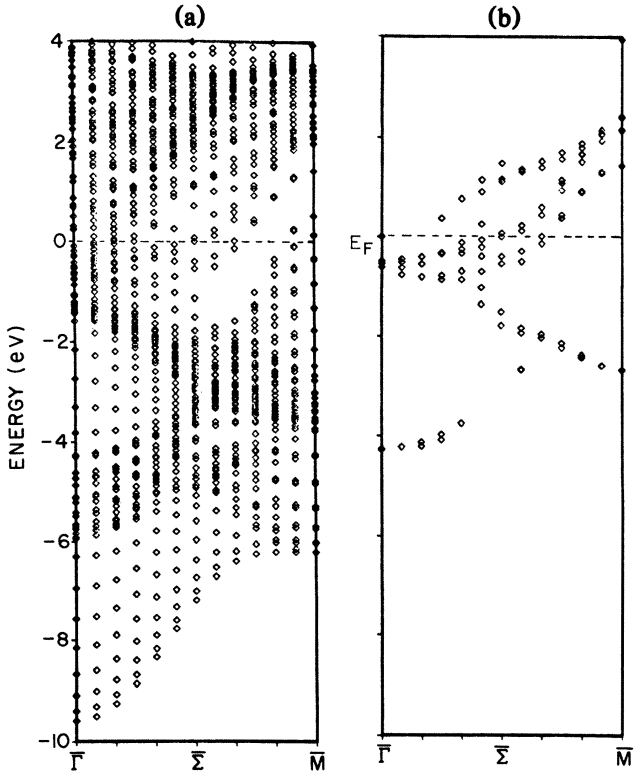


FIG. 7. NTB 19-layer W(001) film (a) energy bands and (b) SR along $\bar{\Sigma}$ (including spin-orbit coupling).

produces a residual cluster of ill-defined SR states at about 0.5 eV below $E_F$.

The limitations of NTB surface-state calculations which are based on bulk band-structure parameters are illustrated in Fig. 6(b). While some SR bands such as C and LL exhibit only modest changes, the remaining bands are more noticeably affected. The principal change is the disappearance of the SH state at $\bar{\Gamma}$. However, it is evident that the energies of other SR states are shifted by amounts that are as large as $0.5-1.0$ eV.

The fully-relativistic NTB energy-band results along $\bar{\Sigma}$ are plotted in Fig. 7(a). Since the fully-relativistic wave function along $\bar{\Sigma}$ contains both even and odd components,[10] it is no long possible to identify states as even or odd and plot them separately as in Figs. 2 and 5. Those fully-relativistic SR states that are 30% localized on a surface layer are shown to the right in Fig. 7(b). The combined effects of finite resonance width and spin-orbit mixing of states with even-odd symmetry yield a cluster of minimally defined SR bands near $E_F$.

As the results in Fig. 7(b) illustrate, a definitive determination of the connectivity and detailed shape of the fully-relativistic SR bands is marginal, even for a moderately thick 19-layer slab. These difficulties become more pronounced in thinner slabs, where the increased resonance widths become comparable to the spin-orbit splitting. In such cases, the usual scalar-relativistic procedure for estimating the SR energy of the semi-infinite crystal in terms of the center of gravity of the appropriate thin-film SR pairs is no longer applicable. This is due to the reduced symmetry of the fully-relativistic wave func-

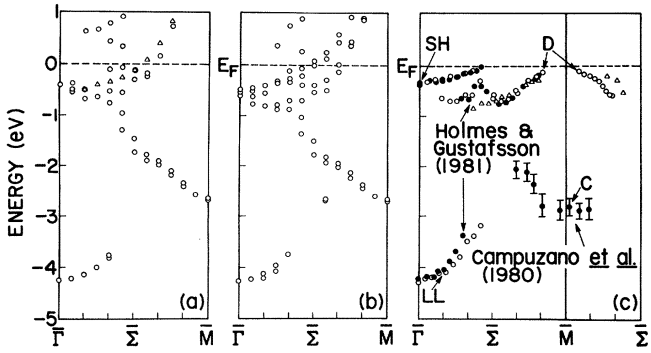


FIG. 8. Comparison of calculated SR dispersion curves along $\bar{\Sigma}$ in the (a) scalar-relativistic and (b) fully-relativistic limits with (c) photoemission data (where the closed and open circles involve photon energies of 18 and 22 eV, respectively).

tion and the difficulty in distinguishing between resonance widths and spin-orbit splittings.

As Grise *et al.*[10] have shown, each scalar-relativistic SR state along $\bar{\Sigma}$ is split into a pair of fully-relativistic SR states, each of which retains a Kramers degeneracy. One must combine the Kramers-degenerate partners to obtain surface states that are localized on one surface or the other. In order to simplify the following discussion, we refer to these spin-orbit-split pairs as a single surface state, using scalar-relativistic terminology. This is appropriate in the present context in view of the finite resonance width that is exhibited by the scalar-relativistic SR bands in Fig. 6. In order to obtain an accurate determination of these spin-orbit splittings, it would be necessary to extend the calculations to even thicker ($\sim$40 layers) films to minimize these resonance widths.

We can best illustrate the manner in which spin-orbit coupling improves the agreement between the calculated and measured SR dispersion curves along $\bar{\Sigma}$ by means of the results shown in Fig. 8. Here we compare the calculated scalar-relativistic and fully-relativistic dispersion curves in Figs. 8(a) and 8(b), respectively, with the experimental points in 8(c) representing ARPES peak positions.[4,5] The even and odd states are superimposed in Figs. 8(a) and 8(c) and the latter are denoted by open triangles.

As anticipated, the principal effect of spin-orbit coupling is to produce a splitting of the nearly-degenerate even-odd doublet bands D. This produces a pair of reasonably-well defined SR bands with features that are in better agreement with the ARPES data in Fig. 8(c). One aspect of this improvement is reflected in the $E_F$-crossing points of the calculated and observed SR bands. The scalar-relativistic crossings in Fig. 8(a) occur at $0.56\bar{M}$ and $0.65\bar{M}$, those for the fully-relativistic results in Fig. 8(b) correspond to $0.49\bar{M}$ and $0.68\bar{M}$, while the experimental values are $0.42\bar{M}$ and $0.88\bar{M}$, respectively. More important, however, is the reinterpretation of the number and identity of the experimental bands discussed below. We note that spin-orbit coupling produces negligible changes in the lower-energy SR bands LL and C, respectively, both of which are in satisfactory agreeement with experiment.

A scalar-relativistic interpretation of the ARPES data near $E_F$ in Fig. 8(c) implies the existence of three SR bands, including SH, D(even), and D(odd). However, the fully-relativistic NTB results in Fig. 8(b) suggest an alternative explanation involving only two bands. These evolve from the spin-orbit-split D(even)-D(odd) doublet. According to this fully-relativistic interpretation, the polarization dependence of the lower branch of the ARPES data is due to the even and odd components of a single SR band, one which possesses a significant admixture of both even and odd character.

The D SR band (or bands) has an important bearing on the physics of this surface. Krakauer *et al.* have computed the wave-vector–dependent susceptibility of the surface and have associated a peak at $\bar{M}$ with the mechanism driving the low-temperature reconstruction.[6] Computationally, this peak arises from the nesting of the SR Fermi surface with its image translated by $\bar{M}$, and the nesting depends on the fact that these bands cross $E_F$ at approximately $\frac{1}{2}\bar{M}$. Holmes and Gustafsson[5] find that the band(s) cross $E_F$ near $\bar{M}$, which casts doubt on this proposed mechanism for the reconstruction. As noted above, the present relativistic results move the $E_F$ crossing point for one mixed even-odd band to $0.68\bar{M}$, in better agreement with experiment.

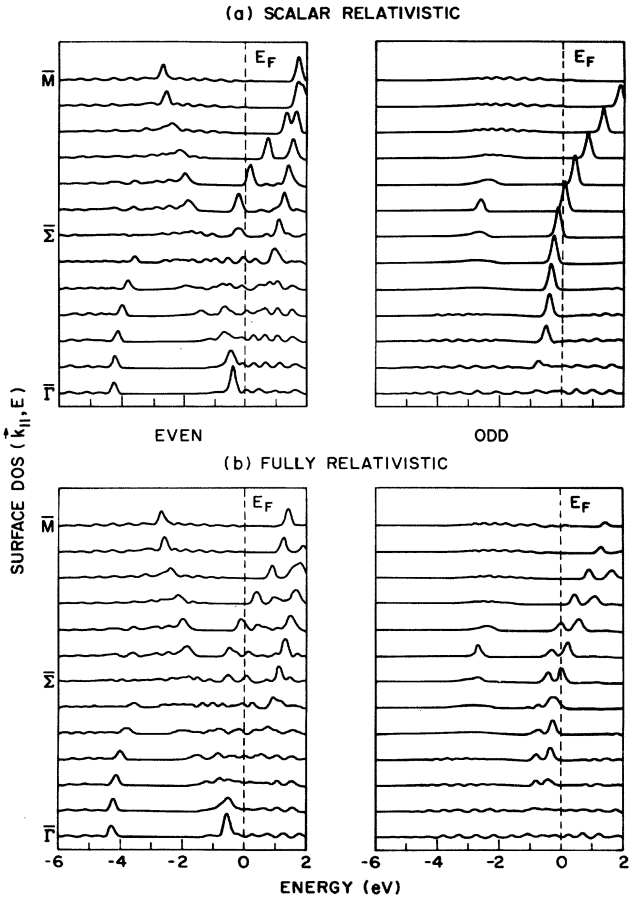


FIG. 9. Wave-vector dependence of the even and odd components of the $\vec{k}_{||}$-resolved NTB surface DOS along $\bar{\Sigma}$ with spin-orbit terms (a) neglected and (b) included.

The question of whether one SR band or two cross $E_F$ near $\bar{M}$ has another important consequence. If experiment is interpreted as showing *two* nearly-filled SR bands, which then contain nearly four electrons per surface atom, the net surface charge is much greater than that predicted by the self-consistent scalar-relativistic calculations. The intuitive concept that near-perfect charge neutrality is attained at metal surfaces, as well as the excellent agreement between the theoretical and experimental work functions, are at odds with this interpretation. The relativistic results provide an alternative: If the experimental D feature is reinterpreted as a single band (per spin) as discussed, this plus the experimental band labeled SH should contain approximately the correct total charge. (We recall that the relativistic SR band corresponding to this feature is in fact the other band arising from the even-odd doublet and does not connect to the orbitally distinct SH state at $\bar{\Gamma}$.)

This difficulty in establishing the symmetry and degeneracy of SR bands in fully-relativistic systems such as W(001) films suggests an alternative way of presenting theoretical results for comparison with experiment. This involves a plot of the $\vec{k}_{||}$-resolved surface DOS. Such a plot is shown in Fig. 9. Here, the energy levels at individual $\vec{k}_{||}$ points along the $\bar{\Sigma}$ line are weighted by the squares of the even and odd projections of the NTB wave functions on the surface layer. Each level is smoothed by a Gaussian with FWHM equal to 0.2 eV. Insofar as these curves mimic experimental energy-distribution spectra, the difficulty of assigning unique dispersion relations to SR states near $E_F$ and $\bar{\Gamma}$ is evident. Plots of this type, with perhaps an exponentially decreasing contribution from underlayers, may be useful for intepreting the ARPES energy-distribution curves directly.

In conclusion, we have shown that the addition of spin-orbit coupling modifies the dispersion of the scalar-relativistic LAPW-NTB surface-state bands along $\bar{\Sigma}$ and provides satisfactory agreement with the high-resolution ARPES data of Campuzano *et al.*[4] and Holmes and Gustafsson.[5] The overall level of agreement is comparable to the differences exhibited by the two independent ARPES measurements. It is useful, nevertheless, to review some possible sources for the remaining discrepancies.

One possibility which has been mentioned above concerns the presence of geometric distortions at room temperature on the W(001) surface. The calculations assume that this surface consists of an ordered $p(1\times1)$ termination of the bulk. However, high-energy ion-scattering data[9] suggest the possibility of a disordered room-temperature phase involving randomized surface-atom displacements parallel to the surface which are characteristic of the low-temperature $c(2\times2)$ reconstruction.

A second effect which could modify the detailed shape of the calculated SR dispersion curves is the energy dependence of $\xi_{6p}$. As noted in Sec. II B, a limited analysis of bulk spin-orbit splittings in terms of the fully-relativistic NTB model suggests a possible energy dependence in $\xi_{6p}$ which has been neglected in the present calculations.

## ACKNOWLEDGMENTS

We are pleased to acknowledge valuable discussions with E. I. Blount, S. D. Kevan, N. V. Smith, and W. Weber on various aspects of this investigation. We are especially grateful to N. V. Smith for suggesting the possible importance of spin-orbit effects on the W(001) surface states and to E. I. Blount for informative conversations concerning surface-state properties in fully-relativistic systems.

[1]M. Posternak, H. Krakauer, A. J. Freeman, and D. D. Koelling, Phys. Rev. B 21, 5601 (1980).
[2]Shang-Lin Weng, E. W. Plummer, and T. Gustafsson, Phys. Rev. B 18, 1718 (1978).
[3]L. W. Swanson and L. C. Crouser, Phys. Rev. Lett. 16, 389 (1966).
[4]J. C. Campuzano, D. A. King, C. Somerton, and J. E. Inglesfield, Phys. Rev. Lett. 45, 1649 (1980).
[5]M. I. Holmes and T. Gustafsson, Phys. Rev. Lett. 47, 443 (1981).
[6]H. Krakauer, M. Posternak, and A. J. Freeman, Phys. Rev. Lett. 43, 1885 (1979).
[7]J. E. Inglesfield, J. Phys. C 12, 149 (1979).
[8]M. Posternak, H. Krakauer, and A. J. Freeman, Phys. Rev. B 25, 755 (1982).
[9]I. Stensgaard, L. C. Feldman, and P. J. Silverman, Phys. Rev. Lett. 42, 247 (1979).
[10]W. R. Grise, D. G. Dempsey, L. Kleinman, and K. Mednick, Phys. Rev. B 20, 3045 (1979).
[11]D. R. Hamann, Phys. Rev. Lett. 46, 1227 (1981).
[12]D. R. Hamann, L. F. Mattheiss, and H. S. Greenside, Phys. Rev. B 24, 6151 (1981).
[13]O. K. Andersen, Phys. Rev. B 12, 3060 (1975); O. Jepsen, J. Madsen, and O. K. Andersen, *ibid.* 18, 605 (1978).
[14]W. M. Walsh and C. C. Grimes, Phys. Rev. Lett. 13, 523 (1964).
[15]L. F. Mattheiss and R. E. Watson, Phys. Rev. Lett. 13, 526 (1964); L. F. Mattheiss, Phys. Rev. 139, A1893 (1965).
[16]N. E. Christensen and B. Feuerbacher, Phys. Rev. B 10, 2349 (1974).
[17]L. F. Mattheiss and W. Weber, Phys. Rev. B 25, 2248 (1982).
[18]D. M. Bylander and L. Kleinman, Phys. Rev. B 27, 3152 (1983).
[19]E. Wigner, Phys. Rev. 46, 1002 (1934).
[20]A. Baldereschi, Phys. Rev. B 7, 5212 (1973); D. J. Chadi and M. L. Cohen, *ibid.* 8, 5747 (1973); H. J. Monkhorst and J. D. Pack, *ibid.* 13, 5188 (1976).
[21]O. K. Andersen, Phys. Rev. B 2, 883 (1970).
[22]I. Tamm, Z. Phys. 76, 849 (1932); Phys. Z. Sowjetunion 1, 733 (1932).
[23]W. Shockley, Phys. Rev. 56, 317 (1939).
[24]S. G. Davidson and J. D. Levine, in *Solid State Physics,* edited by H. Ehrenreich, F. Seitz, and D. Turnbull (Academic, New York, 1970), Vol. 25.
[25]R. L. Billington and T. N. Rhodin, Phys. Rev. Lett. 41, 1602 (1978).